

Article

Uranium Occurrence State and Its Implication for Sandstone-Type Uranium Mineralization within the Hanbazhai Area of the Longchuanjiang Basin, China

Yu Xia ^{1,2,3,*} , Chuanlong Mou ^{1,2,*} and Hao Wu ²

¹ College of Earth Science and Engineering, Qingdao Campus, Shandong University of Science and Technology, Qingdao 266590, China

² Chengdu Center of Geological Survey, China Geological Survey, Ministry of Natural Resources, Chengdu 610081, China; wuhaocgs@sohu.com

³ Key Laboratory of Sedimentary Basin and Oil and Gas Resources, Ministry of Natural Resources, Chengdu 610500, China

* Correspondence: neutron_xy@163.com (Y.X.); chuanlongmu@126.com (C.M.)

Abstract: The Mangbang Formation in the Hanbazhai area is part of the uranium ore field in the Longchuanjiang Basin, China. Uraniferous sandstones from this formation are examined in this study. The type and mode of occurrence of uranium are investigated in detail using an experiment for the sequential extraction of uranium, as well as an electron probe, scanning electron microscopy, and energy spectrum analyses. The sequential extraction experiment indicates that the proportion of uranium minerals is significantly greater than that of the adsorbed uranium in the samples, with the latter being largely present in framboidal pyrites and clay minerals. The results show that these uranium minerals are mainly composed of coffinite and uranium phosphosilicates, which closely coexist with framboidal pyrites, carbon debris, feldspar minerals, and clay minerals. The discovery of coffinite and uranium phosphosilicates is discussed in context with their symbiotic relationship and geochemical environment. Uraniferous sandstones are considered to have undergone at least two stages of mineralization: the sedimentary–diagenetic stage and the later uranium enrichment by fluid. The geochemical environment of the sedimentary–diagenetic stage is generally a sulfide-reducing environment, and the later fluids are rich in U, Si, P, and Y.

Keywords: Longchuanjiang Basin; sandstone-hosted uranium deposit; uranium occurrence state; Hanbazhai area; uranium mineralization



Citation: Xia, Y.; Mou, C.; Wu, H. Uranium Occurrence State and Its Implication for Sandstone-Type Uranium Mineralization within the Hanbazhai Area of the Longchuanjiang Basin, China. *Minerals* **2023**, *13*, 1037. <https://doi.org/10.3390/min13081037>

Academic Editor: Bernard Hubbard

Received: 12 June 2023

Revised: 15 July 2023

Accepted: 30 July 2023

Published: 3 August 2023



Copyright: © 2023 by the authors. Licensee MDPI, Basel, Switzerland. This article is an open access article distributed under the terms and conditions of the Creative Commons Attribution (CC BY) license (<https://creativecommons.org/licenses/by/4.0/>).

1. Introduction

Research on the uranium occurrence state can help to form systematic knowledge not only of the metallogenic process and uranium enrichment mechanism but also of the benefits and metallurgical technology of uranium mining [1]. There are four principal mechanisms accounting for uranium precipitation and fixation in sediments: reduction of uranyl ions to uranous ions; precipitation of insoluble uranyl compounds; absorption on material; and substitution for other elements with similar ionic radii and charges [2]. Uranium ore deposits with organic matter-rich sediments have been identified and occur in lignite with low maturity [3–8]. Previous research has revealed the mechanism for uranium sorption to lignite surfaces in reducing environments [9–12]. A variety of minerals and related phases, including clays, display these same adsorption phenomena [13,14], but the adsorption ability of uranium in clay in the oxidation zone often seems to be larger than that in the reducing area [15–18]. Additionally, uranium (VI) under reducing conditions can form uranium (IV) species, which are often uraninite and coffinite, and can also coprecipitate with framboids of pyrite and carbonate or phosphate minerals [19–21].

With the development of analytical techniques and methodology, the co-occurrence between uranium and other minerals in sandstone-type uranium ore has been evaluated in considerable detail.

Studies of uranium occurrence states in China have mainly focused on Mesozoic to Cenozoic sandstone-type uranium deposits belonging to northern continental sedimentary basins, such as the Ordos Basin and the Erlian Basin [1,22]. The uranium deposit characteristics in the Hanbazzhai area of the Longchuanjiang Basin, South China, have not previously been subject to comprehensive examination. Therefore, energy-dispersive spectrometry (EDS), scanning electron microscopy (SEM), electron probe microanalysis (EPMA), and a sequential extraction procedure are used to (1) identify the degree and occurrence state of uranium enrichment; and (2) probe the mechanism for uranium remobilization, migration and mineralization of the newly obtained uranium ore bodies in the area.

2. Geological Setting

2.1. The Longchuanjiang Basin

The basin is in the Cenozoic basin of the continental borderland in the active Tengchong zone, which is situated in the eastern suture line of Gondwana and the Yangtze plate, and the basin is one of the essential parts of the east Tethyan belt [23]. Tens of small Cenozoic basins are similar to the Longchuanjiang Basin, they have the same geological structural settings, and they are dispersedly distributed in western Yunnan. The basin is one of the essential in situ leachable uranium deposit zones in China, and it possesses multiple uranium deposits, such as No. 381, No. 382, and No. 506. As early as 1987, a uranium extraction test by in situ leaching was carried out successfully in the No. 381 uranium deposit.

The Longchuanjiang Basin is approximately 110 km long from north to south and 0.6–9 km wide from east to west, with an area of approximately 700 square km and a relative elevation difference of 300–500 meters, and it has river valleys and hills as its geomorphology [24]. The basin is an asymmetrical graben controlled by a basement fault. The eastern margin and basement of the basin are mainly deep metamorphic rocks of the Mesoproterozoic Gaoligongshan Group (Pt₂gl). The lithologies of the rocks are feldspathic schist, gneiss and banded migmatite. Medium- to coarse-grained biotite granite is exposed in the western margin and is associated with extensional fault structures and alteration of the late Yanshanian and Himalayan movements. Carboniferous dolomitic limestone and quartz schist are also sporadically exposed in the basin. The Longchuanjiang Basin contains Cenozoic clastic sediments. During the Paleogene to Neogene, the Nanlin and Mangbang (N₂m) Formations were deposited due to extensive subsidence, resulting in mainly terrigenous and volcanoclastic rocks [25] (Figure 1).

Most of the uranium deposits in the Longchuanjiang Basin are in the western gentle slope belt of the margin. Uranium ore bodies occur in the alluvial fan sedimentary system sandstone of the Neogene Mangbang (N₂m) Formation. The ore bodies show shallow burial depths, generally 0–250 m, and take stratoid or lentoid forms. The ore bodies are in a stable aquifer in the groundwater runoff area of the basin. These aquifers have thicknesses of 10–60 m and permeability coefficients of 0.06–0.85 m/d. At the top and bottom of uranium ore bodies, there are more stable confining beds. Based on the previous study of the ore-forming age and diagenetic time, most sandstone-type uranium deposits in the basin are classic epigenetic ores.

2.2. The Hanbazzhai Uranium Deposit

The newly discovered deposit is in the southeastern Longchuanjiang Basin, where the ore body displays a northwest-dipping monocline. We designate the new ore body as No. I. To the southeast, the new deposit borders the No. 506 deposit and was discovered by the China National Nuclear Corporation.

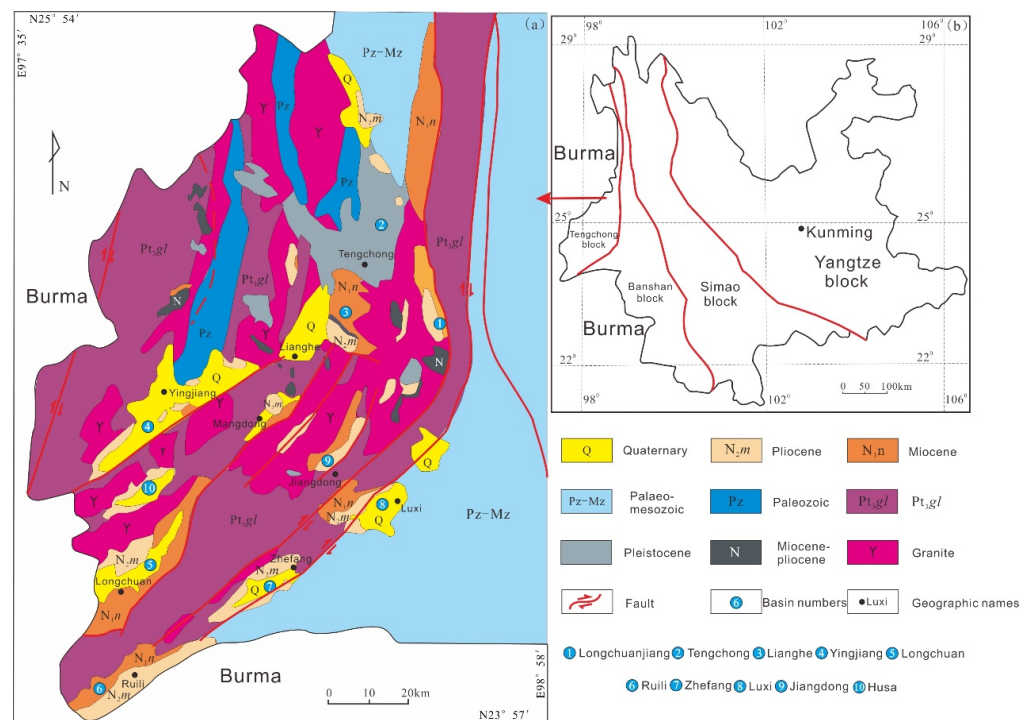


Figure 1. Tectonic setting and geological sketch map of the Tengchong block. (a) Geological sketch map the Tengchong block; (b) Tectonic setting map and simplified location map in Yunnan, China.

The No. I ore body occurs in the lower member of the Neogene Mangbang (N_2m) Formation within the alluvial fan body, which has been drilled by seven drilling projects. The lithologies of mineralized rocks are conglomeratic sandstone and sandy conglomerate. The ore body area is approximately 1.5 square kilometers. The specific features of the No. I ore body are burial depths between 40 and 180 m and bedded or nearly bedded shapes. The occurrence of the ore body is consistent with the occurrence of the rock layer, which has a strike angle of 305° , dip direction angle of 35° and dip angle between 0 and 15° . The average thickness of the ore body is 4.51 m, the maximum thickness is 6.50 m, and the minimum thickness is 0.65 m. We use the lowest grade, which reaches 0.01%, as an estimation standard. The average ore quality of the ore body is 0.0168%, and the highest grade reaches 0.0803%. The ore body becomes thinner towards the northwestern part of the basin and mostly appears in the lower part of carbonaceous fine sandstone and conglomeratic siltstone. The grade and thickness of the ore body show a positive correlation with the thickness of the carbonaceous layer above the ore body.

The No. I ore-bearing strata are different from the known deposits in this basin. An alluvial fan–fan delta–lake sedimentary system mainly developed in the critical geological survey area. Taking cores from the No. 40ZK28 borehole (Figure 2) as a typical case, the ore-bearing strata are always the conglomeratic braided river facies and are characterized by channel subfacies. Previous studies have shown that the ore-bearing strata of the No. 506 borehole mainly contain debris flow facies at the base of the alluvial fan deposit, while the uranium deposits in the western part of the basin occur in the fan delta distributary channel sediment.

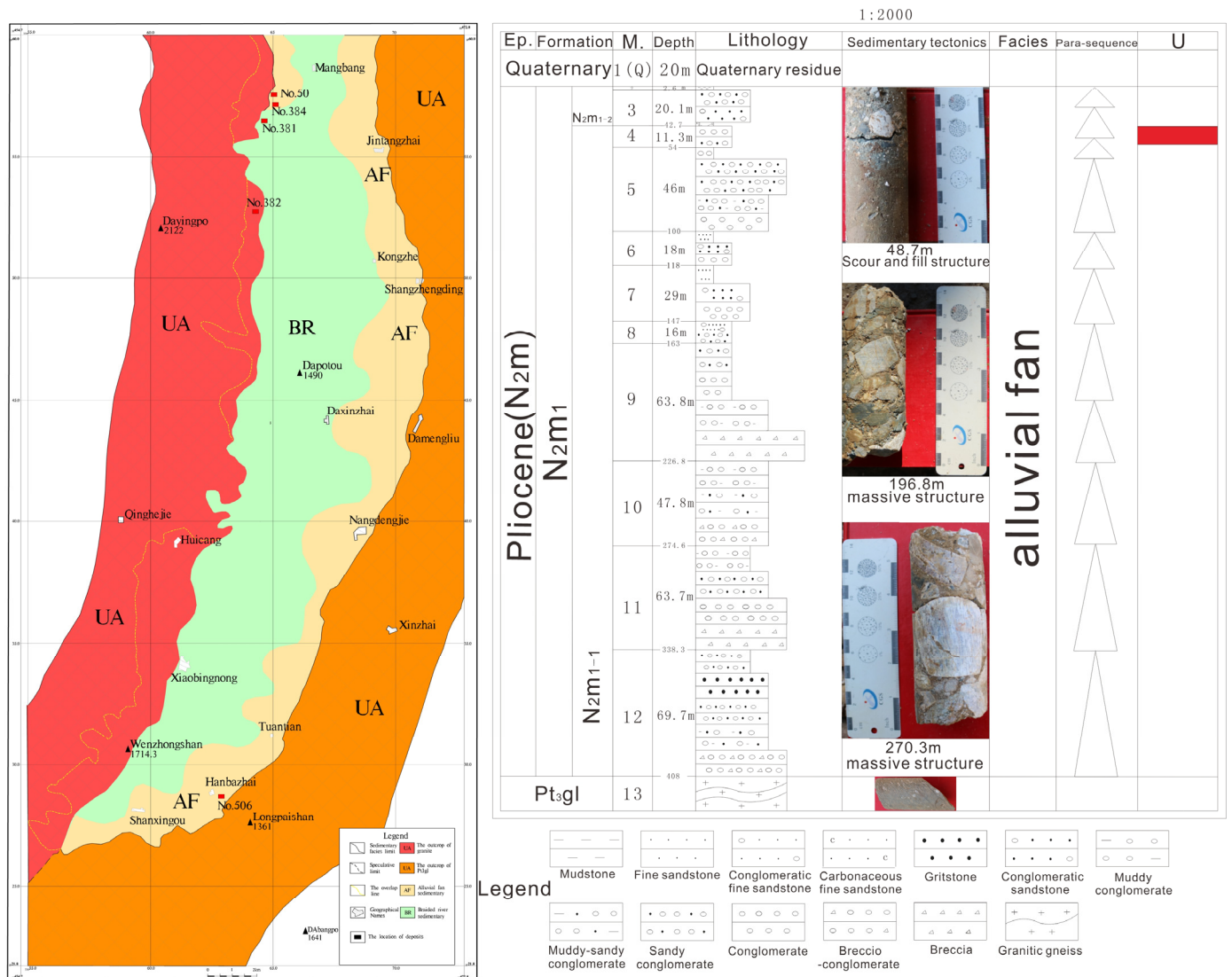


Figure 2. The lithofacies paleogeographic map of the N₂m Formation in the Longchuanjiang Basin and a composite columnar section of the No. 40ZK28 borehole.

3. Samples and Analytical Methods

3.1. Samples

Nineteen mineralized uranium samples in this paper were collected from seven drill holes in the lower segment of the Mangbang Formation in the Hanbazhai uranium deposit and then made into polished thin sections to identify rock textures and mineral assemblages. The samples' properties and measured features are shown in Table 1. The characteristic photographs of thin sections under optical microscopy are shown in Figure 3.

3.1.1. Sandy Conglomerate

The sandy conglomerate has a massive structure and matrix support textures. Its debris grains have poor abrasion and sorting and are subangular–subrounded. The proportion of gravel-sized debris in sandy conglomerate accounts for 70% to 75%, the particle sizes are generally 3–5 mm, and the lithologies are siliceous rocks, schist, granulite, and sericite phyllite. The proportion of sandy debris in sandy conglomerate accounts for 15% to 20%, and the particle sizes are generally 0.1–0.25 mm, with components of single-crystal quartz, potassium feldspar, plagioclase, and rock debris. The interstitial material is composed of clay minerals with contents of less than 5%, which results in a fine-scale cryptocrystalline

texture. The appearances show that iron has impregnated clay minerals, giving the rock its particular brown color.

Table 1. Summary of drill core samples and features measured in this study.

Sample No.	Depth (m)	Lithology	Measurements
30ZK30-06	123.07	Grayish-white sandy conglomerate	Chemical compositions (U 70.5 ppm); EDS and SEM; EPMA
30ZK30-08	119.63	Grayish-white sandy conglomerate	Chemical compositions (U 78.7 ppm); EDS and SEM; EPMA
30ZK30-09	107	Light gray sandy conglomerate	Chemical compositions (U 189 ppm); The sequential extraction procedure
30ZK30-10	107.6	Light gray sandy conglomerate	Chemical compositions (U 223 ppm); The sequential extraction procedure
40ZK28-05	40.5	Grayish-white sandy conglomerate	Chemical compositions (U 430 ppm); The sequential extraction procedure; EDS and SEM
40ZK28-06	41	Grayish-white sandy conglomerate	Chemical compositions (U 459 ppm); The sequential extraction procedure; EDS and SEM
50ZK28-03	161.83	Orange pebbly argillaceous sandstone	Chemical compositions (U 71.1 ppm); EDS and SEM; EPMA
50ZK28-31	148.3	Gray-black carbonaceous sandstone	Chemical compositions (U 184 ppm); The sequential extraction procedure
50ZK28-55	206	Orange pebbly argillaceous sandstone	Chemical compositions (U 1159 ppm); The sequential extraction procedure
10ZK24-04-1	88.22	Grayish white pebbly tuffaceous sandstone	Chemical compositions (U 364 ppm); EDS and SEM; EPMA
10ZK24-04-3	88.22	Grayish white pebbly tuffaceous sandstone	Chemical compositions (U 364 ppm); EDS and SEM; EPMA
10ZK24-07	89.12	Grayish white pebbly tuffaceous sandstone	Chemical compositions (U 1976 ppm); EDS and SEM; EPMA
20ZK10-02	106.35	Grayish white pebbly tuffaceous sandstone	EDS and SEM; EPMA
20ZK10-03	115.4	Grayish-white sandy conglomerate	EDS and SEM; EPMA
20ZK46-01	149.23	Grayish-white tuffaceous sandstone	EDS and SEM; EPMA
20ZK46-02	158.86	Grayish-white sandy conglomerate	EDS and SEM; EPMA
30ZK10-01	130.39	Grayish-white sandy conglomerate	EDS and SEM; EPMA
30ZK10-02	133.06	Grayish-white sandy conglomerate	EDS and SEM; EPMA
30ZK10-03	159.12	Gray pebbly fine sandstone	EDS and SEM; EPMA

3.1.2. Sandstone

The lithology of ore-bearing sandstone is mainly conglomeratic sandstone, and the other lithologies are conglomeratic argillaceous sandstone and carbonaceous sandstone. The gravel contents in pebbly tuffaceous sandstone account for 10% to 20%, and the maximum particle size is up to 5.5 mm, with the lithologies being gneiss, phyllite, siliceous rocks, and sericite metamorphic tuff. The proportion of single-crystal quartz in sandy-size debris accounts for 15% to 20%, feldspar minerals account for 2% to 4.8%, micaceous minerals account for 2.4% to 7.9%, and rock debris accounts for 28% to 49.4% and is

dominated by metamorphic debris. The main substance of interstitial material is volcanic ash, whose rock alterations include kaolinization and hydromicazation.

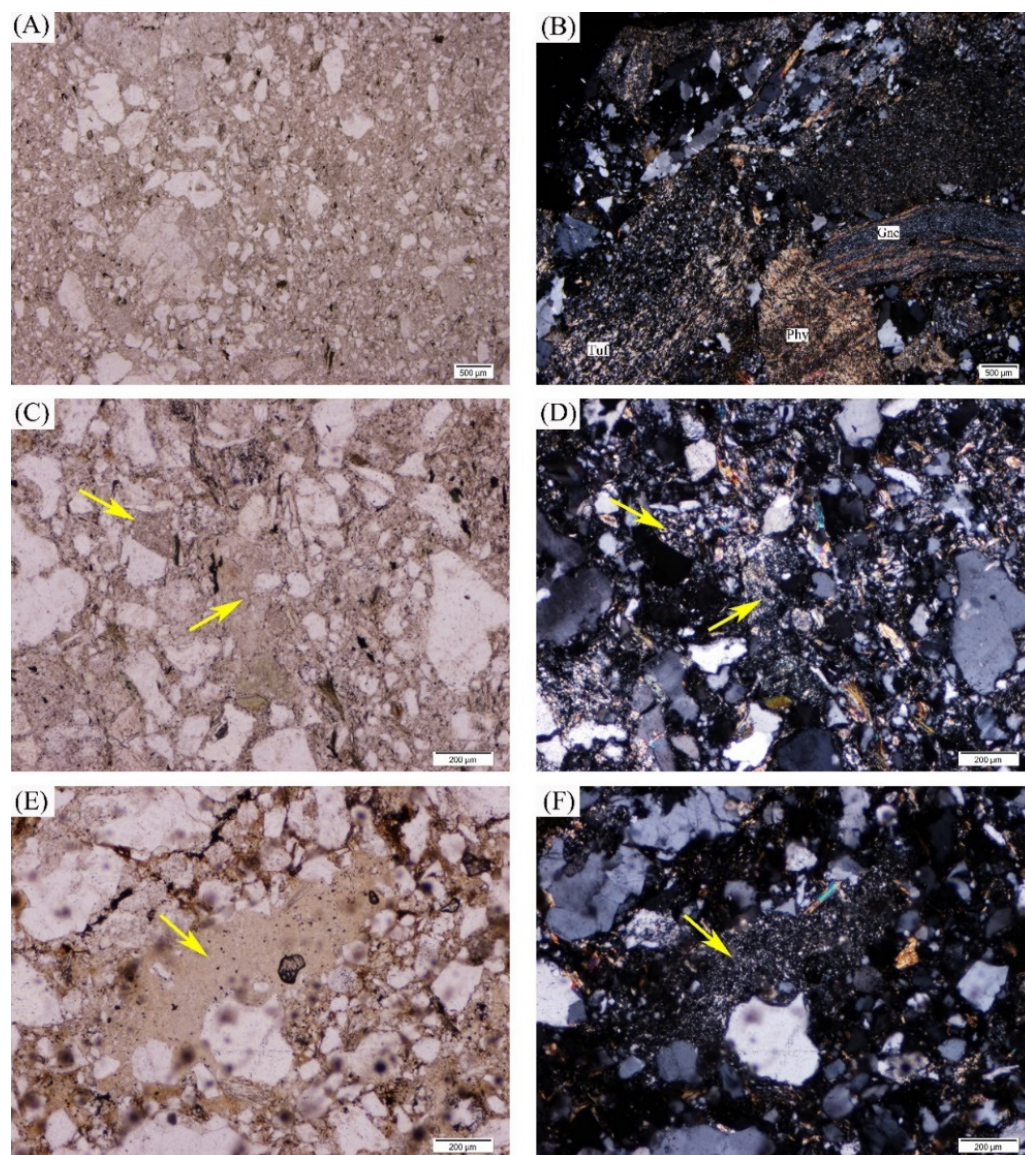


Figure 3. Thin section characteristics under optical microscopy. (A) Pebbly tuffaceous sandstone, 20ZK46-01; (B) rock debris, including Gne = gneiss, Phy = phyllite, and Tuf = sericite metamorphic tuff, 10ZK24-04-1; (C,D) hydromicazation of volcanic ash, in which porosity exists in the form of cavities, 10ZK24-04-2; (E,F) kaolinization of volcanic ash; (C,E) The yellow arrows indicate exist volcanic ash by polarizing microscope with plane polarized light; (D,F) The yellow arrows indicate exist volcanic ash by polarizing microscope with perpendicular polarized light.

The proportion of heavy minerals is less than 1%, and the minerals are garnet, epidote, tourmaline, monazite, zircon, apatite, etc. The ratio of carbonized plant or organic detritus is less than 0.5%, and the distribution is far from uniform.

3.2. Analytical Methods

3.2.1. Optical Microscopy

Optical microscopy (instrument model: Olympus-BX53, which made in Japen; testing environment: indoor temperature of 21 °C; relative humidity of 68%) was used in transmitted and reflected light modes for sample petrographic/mineralogical study, which

was carried out at the Key Laboratory for Sedimentary Basin and Oil and Gas Resources, MLR, China.

3.2.2. EDS and SEM

Scanning electron microscopy (SEM) equipped with an energy-dispersive spectrometer (EDS) was conducted at the Analytical Laboratory, China National Nuclear Corporation (CNNC) Beijing Research Institute of Uranium Geology, and was used to identify the shapes and compositions of the main uranium-bearing phases and establish mineral paragenesis. The instrument model was a Nova Nano SEM450. The operating condition for the SEM was a 15 kV accelerating voltage.

3.2.3. EPMA

In situ EPMA with wave spectrum analysis was conducted at the Analytical Laboratory, CNNC Beijing Research Institute of Uranium Geology, to analyze the elemental composition of uranium minerals. A HEOL JXA-8100 electron microprobe was used at an acceleration voltage of 20 kV, with a beam current of 1×10^{-8} A, a beam spot diameter of 1 μm and an exit angle of 40° . The calibration was made against natural and synthetic oxides or alloys.

3.2.4. Chemical Sequential Extraction Experiment

Tessier method sequential extraction procedures were used to fractionate the uranium in the samples into five geochemical phases and detect the elemental content in each of the following stages: water-soluble, weak acid-extractable, reducible, oxidable, and residual states [26]. The experimental procedures were analogous to those described in the literature [27–29] (Table 2). The chemical sequential extraction experiment was conducted at the Analytical Laboratory, CNNC Beijing Research Institute of Uranium Geology, using a high-resolution–inductively coupled plasma–mass spectrometry (HR–ICP–MS) test method. The testing environment was as follows: the indoor temperature was 21.7°C , and the relative humidity was 43.8%.

Table 2. Chemical sequential extraction procedures.

Occurrence State	The Fractionation Procedures
water-soluble	Take 1 g sample, dissolve in 20 mL distilled water, oscillate 15 min at room temperature, and centrifuge.
weak acid-extractable	Take another 1 g sample, dissolve it in 40 mL acetic acid solution (1 mol/L), oscillated 16 h at room temperature, and centrifuge.
reducible	After washing the solid residue from the previous step, dissolve in 40 mL hydroxylamine hydrochloride solution, oscillated 16 h at room temperature, and centrifuge.
oxidable	After washing the solid residue from the previous step, slowly add in 10 mL H_2O_2 (30 mL) 3 times, oscillate 1 h at 85°C , cool to room temperature, add 50 mL NH_4Ac solution, oscillated 16 h at room temperature, and centrifuge.
residual state	After washing the solid residue from the previous step, add 60°C distilled water in a water bath and evaporate to dryness; after a constant weight is maintained, remove it and perform acid digestions.

4. Results

4.1. Characteristics of the Uranium Contents in Each Geochemical Phase

An HR–ICP–MS test method was used to determine the U contents of six samples by a chemical sequential extraction experiment and by dissolution in a one-step experiment.

The results are shown in Table 3. Overall, the analysis comes to three conclusions: (1) there is no significant difference in the total U contents obtained by the two methods; (2) the contents of uranium in or between the samples show noticeable differences; and (3) the ratio of each U speciation content (the average value) to the total U content (sequential extraction) shows that the residual state (55.59%) > the weak acid-extractable state (21.05%) > the oxidizable state (18.67%) > the reducible state (3.77%) > the water-soluble state (0.82%).

Table 3. Ratio of each U speciation content to the total U content (sequential extraction) and comparison of fractional extraction in samples.

Sample No.	$\omega(\text{U})/\mu\text{g}\cdot\text{g}^{-1}$					Total Contents (Sequential Extraction)	Total Contents (One Step)
	Water-Soluble	Weak Acid-Extractable	Reducible	Oxidizable	Residual		
30ZK30-09	0.65 (0.34%)	22.00 (11.70%)	6.05 (3.22%)	57.30 (30.48%)	102.00 (54.26%)	188.00	189.00
30ZK30-10	1.01 (0.47%)	21.50 (9.63%)	1.58 (0.68%)	140.00 (62.64%)	59.40 (26.58%)	223.49	223.00
40ZK28-05	3.74 (0.87%)	181.00 (42.07%)	27.60 (6.42%)	85.90 (19.96%)	132.00 (30.68%)	430.24	430.00
40ZK28-06	3.87 (0.90%)	158.00 (34.47%)	33.40 (7.28%)	112.00 (24.40%)	151.00 (32.95%)	458.27	459.00
50ZK28-31	1.10 (0.60%)	31.30 (17.11%)	0.99 (0.54%)	77.70 (42.49%)	71.80 (39.26%)	182.90	184.00
50ZK28-55	11.30 (0.97%)	145.00 (12.49%)	17.30 (1.49%)	24.60 (2.12%)	963.00 (82.93%)	1161.20	1159.00
Average value	3.61 (0.82%)	93.13 (21.05%)	14.49 (3.77%)	82.92 (18.67%)	246.53 (55.59%)	442.35	440.67

For the water-soluble state, the metallic ions through adsorption and outer-sphere complexation reactions were non-specifically adsorbed onto the sediment surface and were quickly pulled out by ion exchange with water. As shown in Figure 4 and Table 3, the proportion of uranium in the water-soluble state was very small, which suggested that only a small amount of uranium was adsorbed on the surfaces of clay minerals through diffusion.

The elemental uranium in the weak acid-extractable state was sensitive to pH changes and always occurred in carbonate minerals formed by precipitation or coprecipitation, such as calcite and dolomite, which were extracted with acetic acid; this extraction generally does not destroy iron and manganese oxides or organic matter in the sample [1]. As shown in Figure 4 and Table 3, uranium in the weak acid-extractable state accounted for a high proportion of these samples from borehole 40ZK28, and the ratios of other samples were between 9% and 18%.

In the reducible state, elemental uranium was held in iron oxyhydroxide or manganese oxide by a strong binding force and could be extracted by hydroxylamine hydrochloride solution. The results showed that the uranium in the reducible state accounted for very low amounts, all of which were less than 10%.

In the oxidizable state, elemental uranium was bonded to the organic active groups by adsorption, encapsulation and chelation or adsorbed onto the sulfide particles, which were extracted with hydrogen peroxide solution. Uranium in the weak acid-extractable state accounted for a low proportion in sample 50ZK28-55, but the other samples showed a high level, up to 62.64%, as shown in Figure 4 and Table 3. It was revealed that uranium is closely related to organics and pyrite in this area.

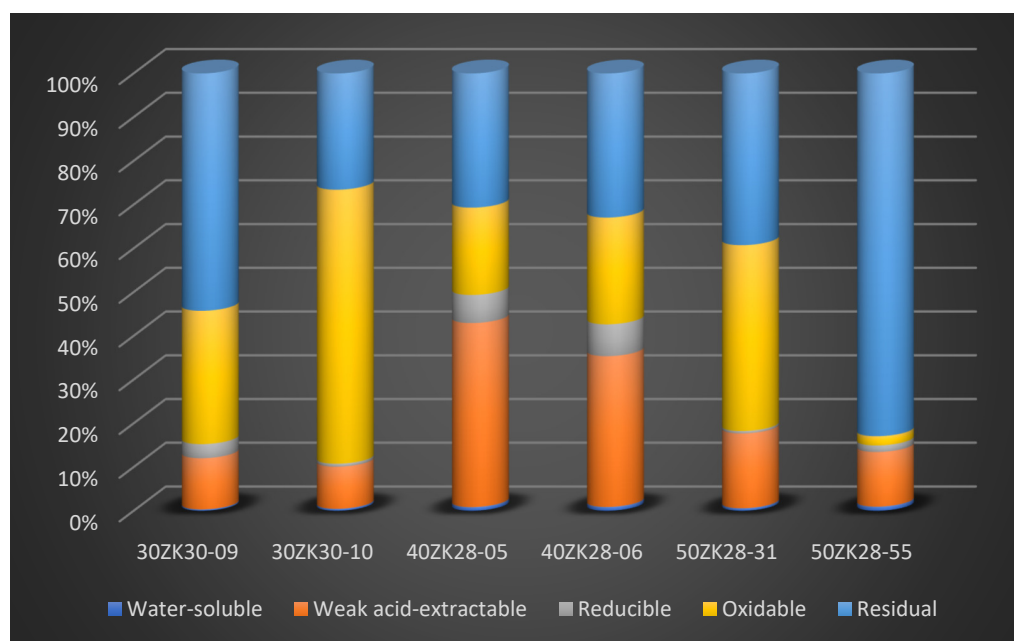


Figure 4. Ratio of each U speciation content to the total U content.

In the residual state, elemental uranium exists in silicate and other stable mineral lattices, with a stable chemical nature, and can be extracted only in a strongly acidic environment. Uranium in the residual state accounted for a high proportion in sample 50ZK28-55, up to 82.93%, and the ratios of other samples were between 26.58% and 54.26%, as shown in Figure 4 and Table 3.

“Active uranium”, also known as “dynamic uranium”, refers to the part with certain migration activity that can be mined by a leaching agent, mainly including adsorbed uranium in the water-soluble state, the weak acid-extractable state, the reducible state, and the oxidable state. As shown in Table 3, the percentage of active uranium in the six samples in this study ranged from 17.07% to 73.24%.

4.2. Types of Uranium Minerals and Their Compositional Analysis

The spatial distribution of the compositional elements in the ore block samples was obtained by backscattering images (Figure 5) spot selection (Table 4) and map analyses (Figure 6, with EPMA. The results indicated that the uranium minerals in the Hanbazhai area were coffinite and uranium phosphosilicates, and the U-bearing minerals were thorite and xenotime [30]. Water is a ubiquitous molecule in uranium minerals [31–34]. Since the electron probe could not detect the characteristic X-rays of hydroxyl and carboxy groups, the total composition could not ultimately reach 100%, but it had no impact on the qualitative discrimination of uranium mineral species.

- (1) As a common mineral, coffinite has shown a close relationship with sandstone-type uranium deposits but rarely appears in the analysis. The composition of coffinite was approximately 50.1%–60.59% UO_2 , 14.32%–17.78% SiO_2 , approximately 4.67%–6.92% P_2O_5 , 1.92%–6.47% CaO , 0.1%–3.85% Al_2O_3 , 0.32%–3.6% FeO and 1.02%–3.7% Y_2O_3 , together with small amounts of K_2O , Na_2O , MgO , TiO_2 , SO_3 , ThO_2 and rare earth elements (REEs). The average UO_2 content was 55.40%, and SiO_2 on average was 15.96%. The data and backscattering image results demonstrated that the contents of UO_2 and SiO_2 in coffinite were low and that impure elements varied widely, probably because coffinite particles were mostly at the submicron–micron level and coffinite is a metamict mineral that easily forms extremely dispersed uraninite and amorphous SiO_2 [35], so the chemical composition of coffinite is susceptible to the effects of symbiotic minerals (quartz, pyrite, feldspar, and clay minerals).

- (2) The composition of thorite was approximately 7.72%–8.79% UO_2 and approximately 53.82%–54.32% ThO_2 , containing small amounts of La and Ce rare earth elements.
- (3) According to the electron probe test data, the study sample probably contained uranium phosphosilicate minerals, which were first reported in the Dalmatovo deposit (West Ural, Russia), which is in an infiltrated buried valley [36]. The composition of this mineral was 9.66%–12.40% P_2O_5 , 4.86%–7.18% CaO, 10.36%–12.51% SiO_2 , and up to 67.81% UO_2 , including almost no iron, which is frequently found in isomorphous varieties of ningyoite and, less commonly, coffinite.
- (4) For monazite, the electron probe results showed that the ThO_2 content was more than 4%, and the UO_2 content was approximately 0.35%.

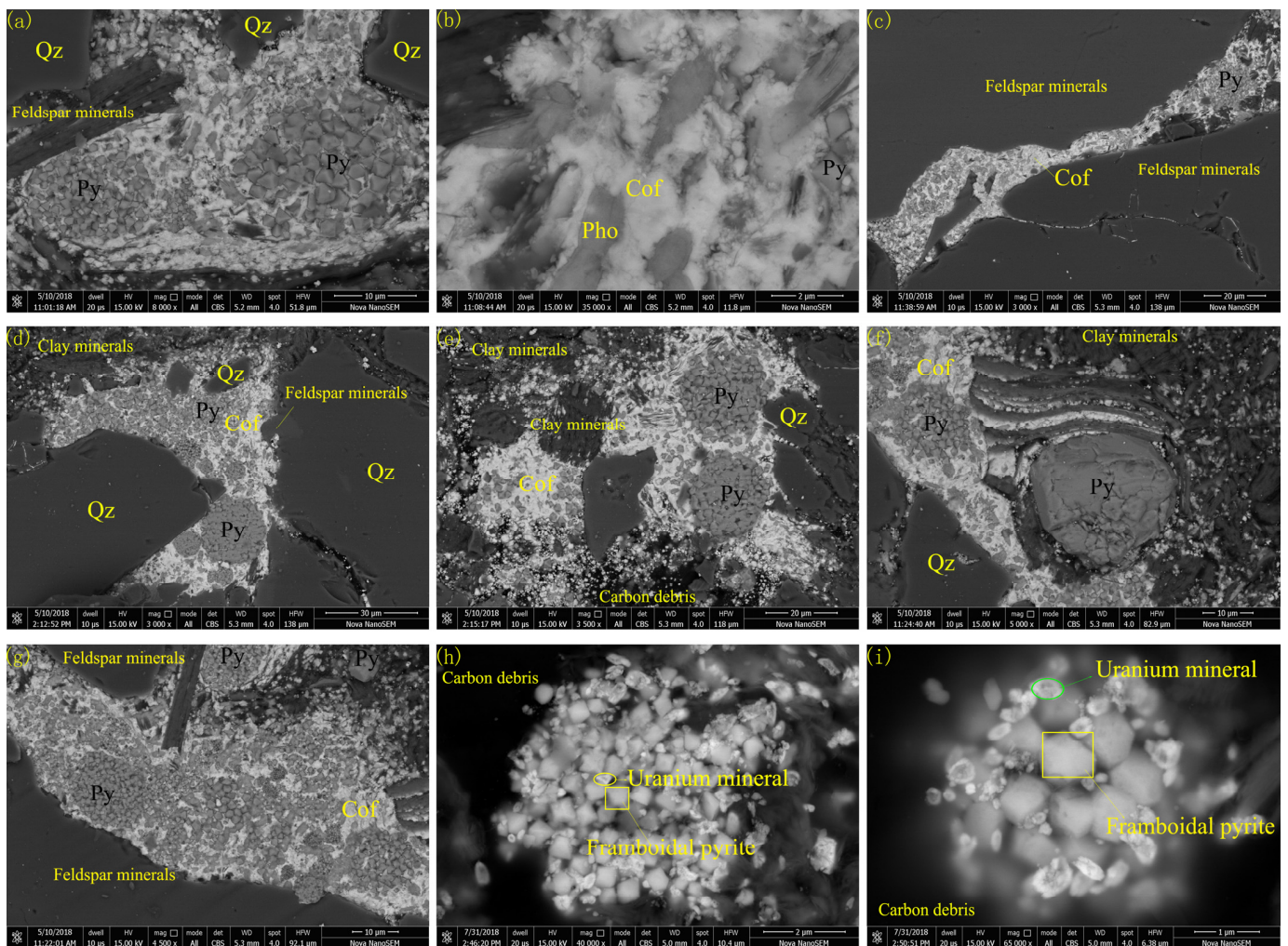


Figure 5. Spatial relationships and microscopic characteristics of the uranium minerals and other minerals; (a) characteristics of framboidal pyrites that are closely associated with uranium minerals; (b) co-occurrence of two uranium minerals; (c) uranium minerals that occur in the fissures of feldspar minerals; (d,e) characteristics of framboidal pyrites that are closely associated with uranium minerals; (f) two different kinds of pyrite; (g) uranium minerals that occur in the fissures of feldspar minerals; (h,i) characteristics of uranium minerals in framboidal pyrite voids. Qz—quartz; Py—pyrite; Cof—coffinite; Pho—uranium phosphosilicates.

Table 4. The electron probe analyses data for uranium minerals in samples.

Sample No.	50ZK28-03					10ZK24-04-1		10ZK24-04-3		10ZK24-07		20ZK10-02		20ZK46-01		30ZK10-02		30ZK30-06
Test Point	1	2	3	4	5	6	7	8	9	10	11	12	13	14	15	16	17	
SiO ₂	16.45	17.78	14.32	14.88	11.25	10.74	10.82	10.36	10.93	11.77	12.51	11.78	10.78	10.77	16.41	20.92	/	
TiO ₂	1.2	0.68	0.53	0.77	/	0.57	0.33	1.06	0.74	0.28	0.45	0.21	0.40	0.50	0.35	/	/	
Al ₂ O ₃	2.01	3.85	2.61	1.8	0.14	0.29	0.17	0.08	0.08	0.29	0.17	0.13	0.31	1.07	0.10	/	/	
FeO	2.34	2.43	3.6	1.35	0.47	0.49	0.28	0.35	0.35	0.98	0.40	2.13	0.61	1.22	0.32	0.16	1.09	
MgO	0.4	0.46	0.81	0.27	0.07	0.12	0.09	0.06	0.11	0.15	0.04	0.04	0.12	0.22	0.15	/	/	
CaO	2.24	1.98	2.32	2.41	4.42	6.32	7.18	5.09	4.86	6.73	6.05	5.83	7.72	7.44	6.47	0.04	0.55	
K ₂ O	0.29	1.64	0.14	0.44	0.11	0.21	0.16	0.19	0.17	0.22	0.21	0.18	0.24	0.32	0.61	0.06	0.03	
Na ₂ O	0.15	0.23	0.19	0.15	0.13	0.11	0.06	/	/	/	/	/	/	/	/	/	/	
P ₂ O ₅	4.99	4.67	5.35	5.49	9.46	11.96	12.40	11.24	11.35	11.92	9.66	10.61	14.03	15.70	6.92	0.59	28.58	
SO ₃	0.24	0.14	0.24	0.17	0.24	0.10	0.18	/	0.05	0.12	0.13	4.83	0.55	2.54	0.06	/	/	
UO ₂	57.88	50.1	57.16	60.59	8.79	65.48	63.81	65.61	67.81	63.59	65.17	60.84	61.81	58.11	51.29	7.72	0.35	
PbO	/	/	0.09	0.29	0.18	0.08	0.1	/	/	/	/	/	/	/	/	/	/	
MnO	/	/	/	/	/	0.32	/	0.28	0.35	0.25	0.15	0.18	0.28	0.11	/	/	/	
V ₂ O ₃	/	/	/	/	/	/	/	/	/	/	/	/	/	/	0.09	0.12		
ThO ₂	1.2	0.68	0.53	0.77	54.32	/	/	/	/	/	/	/	/	/	3.85	53.82	4.07	
ZrO ₂	/	/	/	/	/	/	/	/	/	/	/	/	/	/	/	1.14		
La ₂ O ₃	/	0.23	0.24	/	/	/	/	/	/	/	/	/	/	/	/	/	12.3	
Y ₂ O ₃	3.15	3.04	3.7	3.4	2.57	0.58	0.64	0.57	0.69	0.54	0.45	0.43	0.67	0.69	1.02	1.01	0.93	
Ce ₂ O ₃	0.41	0.51	0.43	/	0.44	0.39	0.27	/	0.21	0.40	0.25	/	0.69	0.22	0.26	0.21	29.43	
As ₂ O ₅	/	0.04	/	/	0.18	0.14	/	0.05	0.12	0.04	/	0.09	/	0.07	/	/	/	
Nd ₂ O ₃	/	/	/	/	/	/	/	/	/	/	/	/	/	0.60	0.44	/	9.87	
Pr ₂ O ₃	/	/	/	/	/	/	/	/	/	/	/	/	/	0.12	/	/	2.97	
Sm ₂ O ₃	/	/	/	/	/	/	/	/	/	/	/	/	/	/	/	/	2.37	
Gd ₂ O ₃	/	/	/	/	/	/	/	/	/	/	/	/	/	/	/	/	1.65	
Eu ₂ O ₃	/	/	/	/	/	/	/	/	/	/	/	/	/	/	/	/	0.19	
Dy ₂ O ₃	/	/	/	/	/	/	/	/	/	/	/	/	/	/	/	/	0.46	
Er ₂ O ₃	/	/	/	/	/	/	/	/	/	/	/	/	/	/	/	/	0.34	
Tm ₂ O ₃	/	/	/	/	/	/	/	/	/	/	/	/	/	/	/	/	0.14	
Total	91.88	88.14	91.83	92.01	92.88	97.9	96.49	94.94	97.82	97.28	95.64	97.28	98.21	99.70	88.34	85.79	95.32	
Type of uranium mineral	coffinite				thorite			uranium phosphosilicates					coffinitethorite		monazite			

4.3. Microscopic Morphology and Symbiotic Relationship of Uranium Minerals

4.3.1. SEM Profiles of Uranium Minerals and Other Minerals

To examine the micromorphology and the spatial relationships of the dominant uranium mineral with other minerals, SEM was used to analyze the ore-bearing sandstones (Figure 5). The observed forms of uranium minerals are (1) uranium minerals associated with framboidal pyrites; (2) two different uranium minerals present together, identified based on electron microprobe data as coffinite and uranium phosphosilicates (Figure 7); (3) uranium minerals distributed along the fissures of feldspar minerals and found in clastic interstitial materials; (4) clay minerals that are closely associated with uranium minerals, and it is speculated that the clay minerals are altered by feldspar minerals; and (6) uranium minerals that formed in framboidal pyrite voids (Figure 5h,i).

4.3.2. Chemical Information of the Uranium Minerals

The study on the rocks in the mineralized section shows that there are U- and Th-rich xenotimes, with UO₂ contents up to 15.59% and ThO₂ contents up to 6.98%. To further explore the relationship between U and Y and Th, EDS area scans of relevant elements were performed (Figure 7). The results show that U is evenly dispersed in mineral particles

and interstitial materials, which is consistent with the electron probe results. The spatial distributions of U and Y show obvious positive correlations but have little correlation with Th.

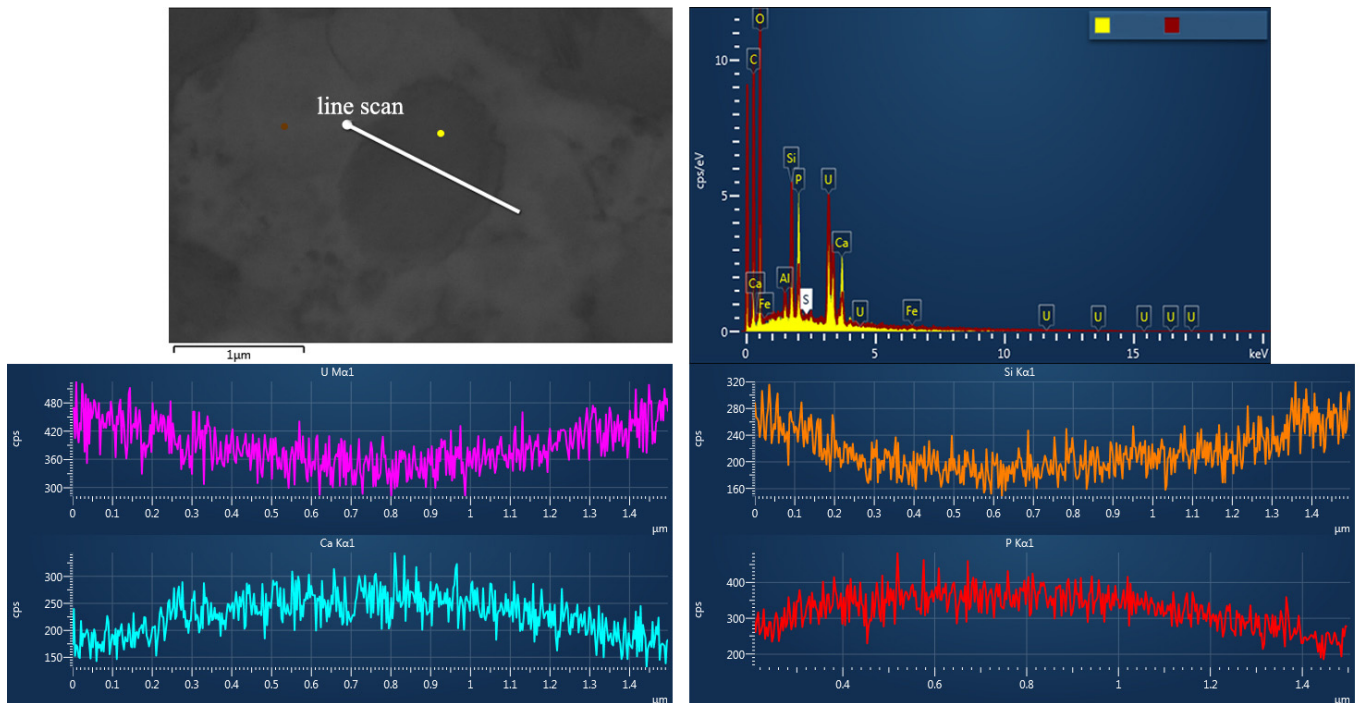


Figure 6. Composition comparison diagram of the two different uranium minerals, with the energy dispersive spectroscopy line scans of relevant elements.

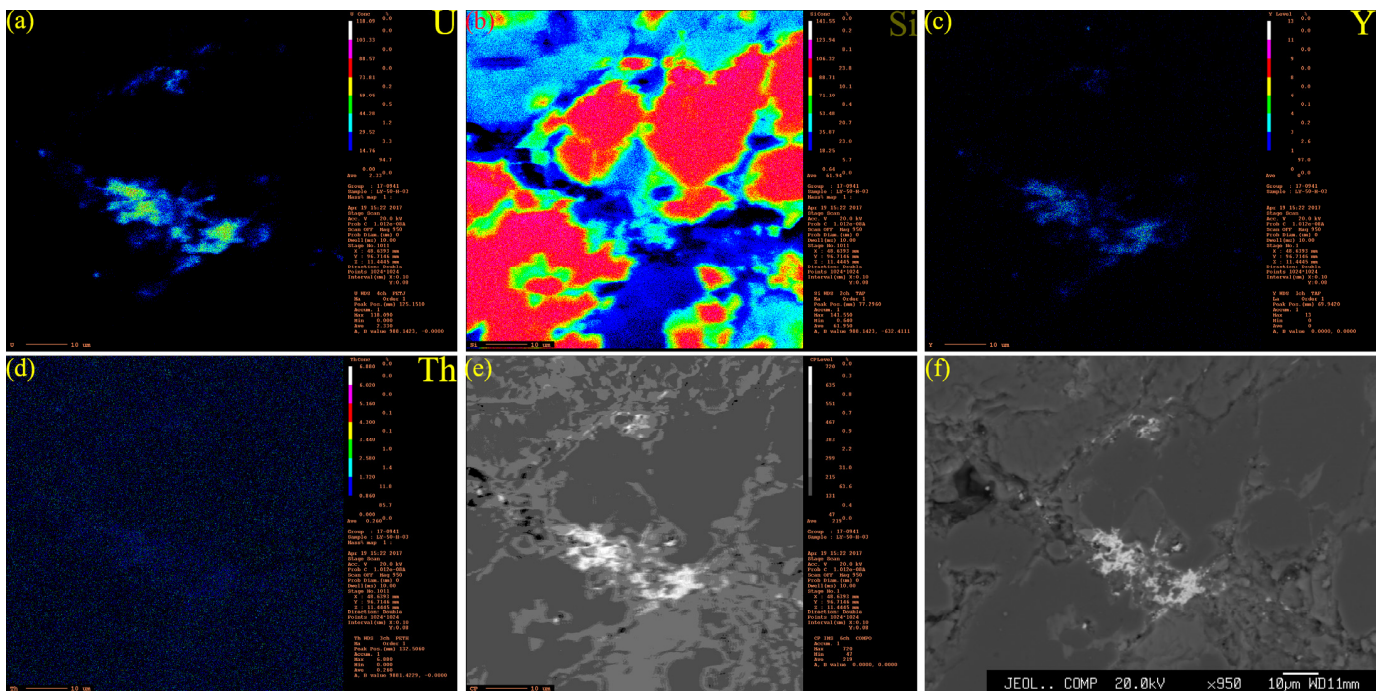


Figure 7. Chemical information of coffinite (e,f), with the EDS area scans of relevant elements (U-(a), Si-(b), Y-(c), and Th-(d)).

5. Discussion

Changes in the oxygen fugacity, pH value, pressure, temperature, and geochemical environment of the surrounding rock can cause uranium precipitation in magma or fluid systems. The reduction of U(6+) to U(4+) is one of the most important mechanisms leading to uranium precipitation [37]. Uranium reduction can occur through biological and abiotic processes. Biological processes reduce uranium mainly by reducing bacteria [38]. The metabolic activities of organic matter and bacteria reduce sulfate to produce hydrogen sulfide and then form metal sulfide. Hydrogen sulfide and Fe(2+) in sulfide are good reducing agents, which are conducive to the reduction and precipitation of uranium [39]. The U(4+) generated by biological process reduction does not always appear as UO₂ but can form complexes with phosphate or carboxylic acid groups, such as CaU(PO₄)₂, U₂O(PO₄)₂, and U₂(PO₄)(P₃O₁₀) [40], which have simple structures and are easily reoxidized and migrated [41]. Abiotic processes generally reduce and precipitate U(4+) by reacting with reducing agents in the fluid. Effective reducing agents include reducing gases, namely H₂, CH₄, CO, H₂S and Fe(II), released from sulfides or biotite alteration [42–44].

5.1. Discussion on the Formation and Genesis of Uranium Minerals in the Study Area

The rock types and assemblage characteristics of host rocks show that the N2m formation in the study area is a set of rapidly deposited strata. The abundant feldspar minerals, volcanic ash, and cuttings in the rocks can provide rich material sources for uranium mineralization in the later stage [45]. The formation of sandstone-type uranium deposits in China is often characterized by multistage superposition and composite genesis [46]. The production characteristics of uranium minerals and their combination with pyrite and other minerals in the study area are diverse, which also shows the multistage formation characteristics of uranium minerals.

5.1.1. Enrichment of Primary Uranium Minerals in the Sedimentary–Diagenetic Stage

The analytical results in Figure 4 show that uranium in the residual state occupies a certain proportion in each sample and is the main component of sample 50ZK28-55. According to previous studies, residual uranium is the most essential component of primary uranium minerals in the sedimentary–diagenetic stage [47]. Figure 8 shows the primary uranium minerals embedded in the quartz particles in the section with ore detritus, indicating that the uranium-bearing detritus particles from the uranium-rich geological bodies in the source area can be rapidly deposited in the basin through transport, forming pre-enriched uranium in the uranium reservoir.

5.1.2. Geochemical Environment of the Sedimentary–Diagenetic Stage

Figure 6 shows that there are framboidal pyrites with different particle sizes in the uranium mineral enrichment area. The framboidal pyrites can be mainly divided into sedimentary and diagenetic types, with the former formed in sulfurized water and the latter formed in anoxic void water in sediments under oxidized or oxygen-poor water (Raiswell and Berner, 1985 [48]), and these pyrites are different in shape, particle size, and sulfur isotopes (Sawlowicz, 2000; Wei et al., 2016 [49,50]). The sedimentary framboidal pyrites have a tiny average particle size and little change in the particle size range ($5.0 \pm 1.7 \mu\text{m}$), while these features are the opposite for diagenetic framboidal pyrites ($7.7 \pm 4.1 \mu\text{m}$) [51–53]. It can be preliminarily determined that the framboidal pyrites in the uranium section are mainly in the sedimentary stage. Additionally, some scholars believe that framboidal pyrites were formed in the sulfate reduction stage of organic matter decomposition (Berner and Raiswell, 1983; Berner, 1984 [54,55]); therefore, it can be concluded that the geochemical environment of the study area during the depositional to diagenetic period was sulfide-reducing.

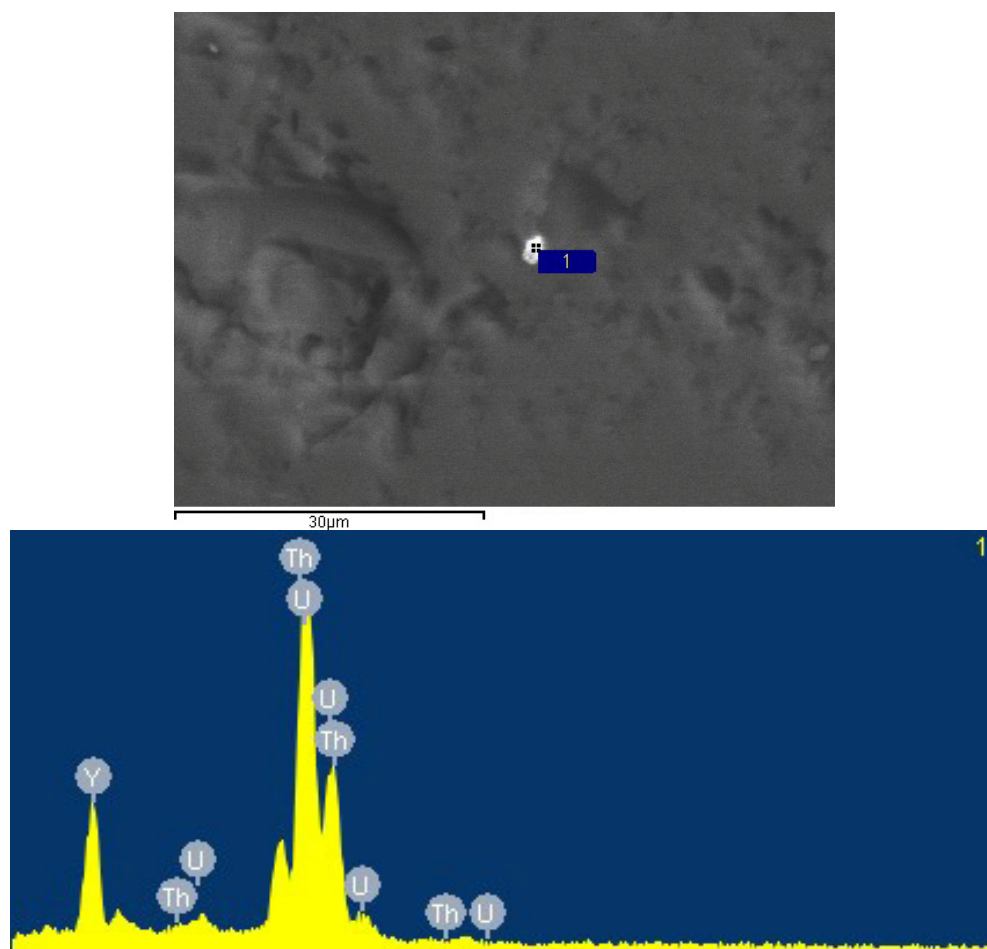


Figure 8. Characteristics and energy spectrum of primary uranium minerals embedded in quartz grains (1 indicates the point position of the energy spectrum).

5.1.3. The Stage of Uranium Enrichment by Later Fluids

The metallogenic characteristics of sandstone-type uranium deposits are closely related to the properties of the later liquids. The process of convergence and mixing to the unloading of fluids with different properties is an essential mechanism for sandstone uranium mineralization. The U(6+) from the outlined source area that has been released in the sedimentary layer participates in uranium mineralization with the flow of oxygen-containing water. When the fluid migrates to the front line of the oxidation zone, U(6+) is reduced to U(4+) [56].

Coffinite is mainly formed in reducing and alkaline environments [57–59]. In terms of mineral composition, P and Y are relatively high in coffinite minerals in this area (Table 4). P-rich coffinite is identical to uranium phosphosilicates in terms of the element type (Figure 7). Some scholars have noted that P-rich coffinite may be a product of the evolution of ningyoite (a kind of uranium phosphosilicate) [60]. P-rich coffinite can also be formed in uranium-containing fluids, in which phosphorus- and silicon-rich and phosphate minerals can lead to the reduction of uranyl precipitation [61,62]. Phosphorus and uranium have strong complexation, and increasing the phosphate concentration strengthens the adsorption of iron minerals to uranium [63–65]. The abundance of phosphorus in uranium minerals is also considered favorable evidence for biomineralization [66,67]. When bacteria degrade organic matter, they can break the chemical bonds in organophosphate esters and release phosphorus [68]. In addition, in the process of bacterial sulfate reduction, bacterial activities can produce organic acids and other substances and reduce the environmental pH value, leading to the dissolution of apatite and other P-rich minerals [69,70].

There is no consensus on the origin of Y enrichment in uranium minerals. U^{4+} and Y^{3+} can undergo heterovalent homomorphic substitution. Ma [47] suggested that the formation of Y-rich coffinite may be related to the action of high-salinity hydrothermal fluid, while Toyoda [71] believed that the enrichment of Y is closely associated with biological phosphate. Regardless of what causes the enrichment of P and Y in coffinite, they all reflect the characteristics of abundant U, Si, P, and Y in the later fluids [72].

5.1.4. The Adsorption of Uranium

In sedimentary rocks, lignite has the strongest adsorption capacity for uranium, followed by phosphorite, limonite, and clay, while pure limestone and sandstone have the weakest adsorption capacity [73]. Feldspar, kaolinite, iron oxide, montmorillonite, and pyrite are also suitable adsorbents for uranium [74]. Generally, the adsorption capacity of minerals with a good crystallization degree and coarse particle size is weak, while the adsorption capacity of various mineral colloids is much stronger. As shown in Figure 6 H-I, some uranium minerals in the study area adsorbed and grew on the surfaces of framboidal pyrites and clay minerals.

6. Conclusions

- (1) By using an experiment to sequentially extract uranium, electron probe microanalysis, scanning electron microscopy and energy spectroscopy indicate that the type and mode of occurrence of uranium in the Hanbazhai area of the Longchuanjiang Basin have adsorbed uranium and uranium minerals, which are closely related to framboidal pyrite, feldspar minerals, clay minerals, and organic matter. Uranium minerals include coffinite and uranium phosphosilicates, and U-rich minerals include thorite and xenotime.
- (2) It is considered that uraniferous sandstones have undergone at least two stages of mineralization: the sedimentary–diagenetic stage and the later uranium enrichment by fluid. The geochemical environment of the sedimentary–diagenetic stage is generally a sulfide-reducing environment, and the later fluids are rich in U, Si, P, and Y.

Author Contributions: Conceptualization, C.M. and Y.X.; methodology, H.W. and Y.X.; software, Y.X.; writing—original draft preparation, Y.X.; writing—review and editing, H.W. and Y.X. All authors have read and agreed to the published version of the manuscript.

Funding: This research was funded by Project of China Geological Survey grant number [DD 20190122; DD20230049; DD20230338] And Project of Gansu Provincial Bureau of Geology and Mineral Exploration & Development [2022 JS-153] and Liubaojun Academician Foundation of Chengdu Center of China Geological Survey (Characteristics of source rocks in Datangpo formation, Sichuan Basin).

Data Availability Statement: No new data were created or analyzed in this study. Data sharing is not applicable to this article.

Conflicts of Interest: The authors declare no conflict of interest.

References

1. Chen, L.; Chen, Y.; Feng, X.; Li, J.-G.; Guo, H.; Miao, P.; Jin, R.; Tang, C.; Zhao, H.; Wang, G.; et al. Uranium Occurrence State in the Tarangaole Area of the Ordos Basin, China: Implications for Enrichment and Mineralization. *Ore Geol. Rev.* **2019**, *115*, 103034. [[CrossRef](#)]
2. Burns, P.C.; Finch, R.J. (Eds.) *Uranium: Mineralogy, Geochemistry, and the Environment*; Walter de Gruyter GmbH & Co KG: Berlin, Germany, 2018.
3. Wu, S.; Wang, D. Uranium concentration by organic matter during diagenesis and mineralization in the continental sandstone-type uranium deposit in North Sichuan. *Uranium Geol.* **1991**, *7*, 265–272, (In Chinese with English Abstract).
4. Alberic, P.; Viollier, E.; Jezequel, D.; Grosbois, C.; Michard, G. Interactions between trace elements and dissolved organic matter in the stagnant anoxic deep layer of a meromictic lake. *Limnol. Oceanogr.* **2000**, *45*, 1088–1096. [[CrossRef](#)]
5. Yang, Z. Occurrence and Abundance of V, Cr, Mo, and U in the Late Permian Coals from Yanshan, Yunnan, China. *Bull. Mineral. Petrol. Geochem.* **2009**, *28*, 268–271, (In Chinese with English Abstract).

6. Cuney, M. Evolution of uranium fractionation processes through time: Driving the secular variation of uranium deposit types. *Econ. Geol.* **2010**, *105*, 553–569. [[CrossRef](#)]
7. Douglas, G.B.; Butt, C.R.M.; Gray, D.J. Geology, geochemistry and mineralogy of the lignite-hosted Ambassador palaeochannel uranium and multi-element deposit, Gunbarrel Basin, Western Australia. *Miner. Depos.* **2011**, *46*, 761–787. [[CrossRef](#)]
8. Hou, H.Q.; Li, Y.R.; Liu, H.J.; Han, S.Y.; Wang, G.; Bai, Y.S.; Wu, B.L. The organic matter characteristics of the Zhiluo Formation and its relationship with uranium mineralization in the North Ordos Basin. *Acta Geol. Sin.* **2016**, *90*, 3367–3374, (In Chinese with English Abstract).
9. Fomina, M.; Charnock, J.M.; Hillier, S.; Alvarez, R.; Gadd, G.M. Fungal transformations of uranium oxides. *Environ. Microbiol.* **2007**, *9*, 1696–1710. [[CrossRef](#)]
10. Cumberland, S.A.; Douglas, G.; Grice, K.; Moreau, J.W. Uranium mobility in organic matter-rich sediments: A review of geological and geochemical processes. *Earth-Sci. Rev.* **2016**, *159*, 160–185. [[CrossRef](#)]
11. Cumberland, S.A.; Etschmann, B.; Brugger, J.; Douglas, G.; Evans, K.; Fisher, L.; Kappen, P.; Moreau, J.W. Characterization of uranium redox state in organic-rich Eocene sediments. *Chemosphere* **2018**, *194*, 602–613. [[CrossRef](#)]
12. Rallakis, D.; Michels, R.; Brouand, M.; Parize, O.; Cathelineau, M. The Role of Organic Matter on Uranium Precipitation in Zoovch Ovoo, Mongolia. *Minerals* **2019**, *9*, 310. [[CrossRef](#)]
13. Whicker, J.J.; Pinder III, J.E.; Ibrahim, S.A.; Stone, J.M.; Breshears, D.D.; Baker, K.N. Uranium partition coefficients (K-d) in forest surface soil reveal long equilibrium times and vary by site and soil size fraction. *Health Phys.* **2007**, *93*, 36–46. [[CrossRef](#)] [[PubMed](#)]
14. Rodriguez, P.B.; Tome, F.V.; Lozano, J.C.; Perez-Fernandez, M.A. Influence of soil texture on the distribution and availability of U-238, Th-230, and Ra-226 in soils. *J. Environ. Radioact.* **2008**, *99*, 1247–1254. [[CrossRef](#)] [[PubMed](#)]
15. Yang, D.; Yu, M. The clay mineral characteristics and the relation to uranium mineralization in Turpan-Hami Basin. *Contrib. Geol. Miner. Resour. Res.* **2005**, *20*, 188–191, (In Chinese with English Abstract).
16. Ohnuki, T.; Yoshida, T.; Ozaki, T.; Samadfam, M.; Kozai, N.; Yubuta, K.; Mitsugashira, T.; Kasama, T.; Francis, A.J. Interactions of uranium with bacteria and kaolinite clay. *Chem. Geol.* **2005**, *220*, 237–243. [[CrossRef](#)]
17. Liu, Z.Y.; Peng, S.P.; Qin, M.K.; Liu, H.X.; Geng, Y.Y.; Zhang, X.; Ding, B.; Xiu, X.Q. Origin and role of kaolinization in roll-front uranium deposits and its response to ore-forming fluids in the Yili basin, China. *Geofluids* **2018**, *2018*, 7847419. [[CrossRef](#)]
18. Wu, D.; Pan, J.; Xia, F.; Huang, G.; Lai, J. The Mineral Chemistry of Chlorites and Its Relationship with Uranium Mineralization from Huangsha Uranium Mining Area in the Middle Nanling Range, SE China. *Minerals* **2019**, *9*, 199. [[CrossRef](#)]
19. Duff, M.C.; Coughlin, J.U.; Hunter, D.B. Uranium co-precipitation with iron oxide minerals. *Geochim. Cosmochim. Acta* **2002**, *66*, 3533–3547. [[CrossRef](#)]
20. Reeder, R.J.; Nugent, M.; Lamble, G.M.; Tait, C.D.; Morris, D.E. Uranyl incorporation into calcite and aragonite: XAFS and luminescence studies. *Environ. Sci. Technol.* **2000**, *34*, 638–644. [[CrossRef](#)]
21. Doinikova, O.A. Uranium deposits with a new phosphate type of blacks. *Geol. Ore Depos.* **2007**, *49*, 80–86. [[CrossRef](#)]
22. Bonnetti, C.; Cuney, M.; Michels, R.; Truche, L.; Malartre, F.; Liu, X.; Yang, J. The multiple roles of sulfate-reducing bacteria and Fe-Ti oxides in the genesis of the Bayinwula roll front-type uranium deposit, Erlan Basin, NE China. *Econ. Geol.* **2015**, *110*, 1059–1081. [[CrossRef](#)]
23. Chen, Y. Discussion on characteristics, genesis type and genetic model of in-situ leachable sandstone type uranium deposits in Western Yunnan. *Uranium Geol.* **1998**, *14*, 193–199, (In Chinese with English Abstract).
24. Yao, Y.; Sun, Z. Geophysical characteristics of strata (rocks) and application of geophysical methods in Longchuanjiang Basin. *Uranium Geol.* **2004**, *20*, 245–250, (In Chinese with English Abstract).
25. Sun, Z.; Chen, H.; Zhu, X.; Wu, Y.; Yang, Y.E. Cenozoic coupled basin-mountain and prospecting direction for sandstone-type uranium deposits in Western Yunnan. *Uranium Geol.* **2007**, *23*, 289–297, (In Chinese with English Abstract).
26. Zhang, C.Y.; Peng, P.A.; Song, J.Z.; Liu, C.S.; Peng, J.; Lu, P.X. Utilization of modified BCR procedure for the chemical speciation of heavy metals in Chinese soil reference material. *Ecol. Environ. Sci.* **2012**, *21*, 1881, (In Chinese with English Abstract).
27. Wan, X.; Wang, W.; Ye, T.M.; Guo, Y.W.; Gao, X.B. A study on the chemical and mineralogical characterization of MSWI fly ash using a sequential extraction procedure. *J. Hazard. Mater. B* **2006**, *134*, 197–201. [[CrossRef](#)]
28. Smeda, A.; Zyrnicki, W. Application of sequential extraction and the ICP-AES method for study of the partitioning of metals in fly ashes. *Microchem. J.* **2002**, *72*, 9–16. [[CrossRef](#)]
29. Sun, Y.; Qi, G.; Lei, X.; Xu, H.; Li, L.; Yuan, C.; Wang, Y. Distribution and mode of occurrence of uranium in bottom ash derived from high-germanium coals. *J. Environ. Sci.* **2016**, *43*, 91–98. [[CrossRef](#)] [[PubMed](#)]
30. Xia, Y.; Zhou, K.; Wu, H.; Chen, X.; Zhang, J.; Kong, R. Uranium mineral occurrence of new sandstone type uranium deposits in Western Yunnan. *Sci. Technol. Eng.* **2018**, *18*, 49–55, (In Chinese with English Abstract).
31. Wei, S. *Chinese Uranium Minerals*; China Atomic Energy Press: Beijing, China, 1979; pp. 65–73. (In Chinese)
32. Min, M.Z.; Zhang, F.S.; Zhao, F.M.; Wang, D.Y. *Genesis of Uranium Mineralogy Studies*; Atomic Energy Press: Beijing, China, 1992; pp. 95–99. (In Chinese)
33. Zhang, J. *Solution Equilibrium of Uranium Minerals*; Atomic Energy Press: Beijing, China, 2008; pp. 156–163. (In Chinese)
34. Zhang, J.Y.; Wang, A.Z.; Li, X.Y.; Zheng, Z.X.; Li, J.Z. *Uranium mineralogy of China*; Atomic Energy Press: Beijing, China, 1995; pp. 3–282. (In Chinese)
35. Li, J.; Chen, Y.; Zhang, C. *A Concise Course on Uranium Geology and Exploration*; Geology Press: Beijing, China, 2011. (In Chinese)

36. Doynikova, O.A.; Sidorenko, G.A.; Sivtsov, A.V. Phosphosilicates of tetravalent uranium. In *Doklady Earth Sciences*; Pleiades Publishing: New York, NY, USA, 2014; Volume 456, pp. 755–758.
37. Yu, Z.Q.; Ling, H.F.; Mavrogenes, J.; Chen, P.R.; Chen, W.F.; Fang, Q.C. Metallogeny of the Zoujiashan uranium deposit in the Mesozoic Xiangshan volcanic-intrusive complex, southeast China: Insights from chemical compositions of hydrothermal apatite and metal elements of individual fluid inclusions. *Ore Geol. Rev.* **2019**, *113*, 103085. [[CrossRef](#)]
38. Wilkins, M.J.; Livens, F.R.; Vaughan, D.J.; Lloyd, J.R. The impact of Fe(III)-Reducing bacteria on uranium mobility. *Biogeochemistry* **2006**, *78*, 125–150. [[CrossRef](#)]
39. Prakash, O.M.; Gihring, T.M.; Dalton, D.D.; Chin, K.J.; Green, S.J.; Akob, D.M.; Wanger, G.; Kostka, J.E. *Geobacter daltonii* sp. nov., an Fe(III)- and uranium(VI)-reducing bacterium isolated from a shallow subsurface exposed to mixed heavy metal and hydrocarbon contamination. *Int. J. Syst. Evol. Microbiol.* **2010**, *60*, 546–553. [[CrossRef](#)] [[PubMed](#)]
40. Bernier-Latmani, R.; Veeramani, H.; Vecchia, E.D.; Junier, P.; Lezama-Pacheco, J.S.; Suvorova, E.I.; Sharp, G.O.; Wigginton, N.S.; Bargar, J.R. Non-uraninite products of microbial U (VI) reduction. *Environ. Sci. Technol.* **2010**, *44*, 9456–9462. [[CrossRef](#)]
41. Latta, D.E.; Kemner, K.M.; Mishra, B.; Boyanov, M.I. Effects of calcium and phosphate on uranium(VI) oxidation: Comparison between nanoparticulate uraninite and amorphous U (VI)- Phosphate. *Geochim. Cosmochim. Acta* **2016**, *174*, 122–142. [[CrossRef](#)]
42. Latta, D.E.; Boyanov, M.I.; Kemner, K.M.; O'Loughlin, E.J.; Scherer, M.M. Abiotic reduction of uranium by Fe(II) in soil. *Appl. Geochem.* **2012**, *27*, 1512–1524. [[CrossRef](#)]
43. Hu, R.Z.; Bi, X.W.; Zhou, M.F.; Peng, J.T.; Su, W.C.; Liu, S.; Qi, H.W. Uranium metallogeny in South China and its relationship to crustal extension during the Cretaceous to Tertiary. *Econ. Geol.* **2008**, *103*, 583–598. [[CrossRef](#)]
44. Dargent, M.; Truche, L.; Dubessy, J.; Bessaque, G.; Marmier, H. Reduction kinetics of aqueous U(VI) in acidic chloride brines to uraninite by methane, hydrogen or C-graphite under hydrothermal conditions: Implications for the genesis of unconformity-related uranium ore deposits. *Geochim. Cosmochim. Acta* **2015**, *167*, 11–26. [[CrossRef](#)]
45. Shamim, A.; Gu, H.; Yang, X. Uranium enrichment in tuff of Upper Triassic in the ordos Basin. *Geol. Rev.* **2016**, 401–402.
46. Zhang, J.; Xu, G.; Lin, J.; Peng, Y.; Wang, G. The implication of six kinds of new sandstone-type uranium deposits to uranium resources potential in North China. *Geol. China* **2010**, *37*, 1434–1449, (In Chinese with English Abstract).
47. Ma, Y.; Wu, B.; Liu, Y.; Liu, C.; Zhao, Z.; Wang, H.; Song, Z.; Wei, A. Study on uranium occurrence state of sandstone-type uranium deposits in HJQ region, Ordos Basin. *Northwestern Geol.* **2013**, *46*, 141–152, (In Chinese with English Abstract).
48. Raiswell, R.; Berner, R.A. Pyrite formation in euxinic and semi-euxinic sediments. *Am. J. Sci.* **1985**, *285*, 710–724. [[CrossRef](#)]
49. Sawlowicz, Z.; Gize, A.P.; Rospondek, M. *Organic Matter from Zechstein Copper Deposits (Kupferschiefer) in Poland//Organic Matter and Mineralisation: Thermal Alteration, Hydrocarbon Generation and Role in Metallogenesis*; Springer: Dordrecht, The Netherlands, 2000; pp. 220–242.
50. Wei, H.Y.; Wei, X.M.; Qiu, Z.; Song, H.; Shi, G. Redox conditions across the G-L boundary in South China: Evidence from pyrite morphology and sulfur isotopic compositions. *Chem. Geol.* **2016**, *440*, 1–14. [[CrossRef](#)]
51. Wilkin, R.T.; Barnes, H.L.; Brantley, S.L. The size distribution of framboidal pyrite in modern sediments: An indicator of redox conditions. *Geochim. Cosmochim. Acta* **1996**, *60*, 3897–3912. [[CrossRef](#)]
52. Garciaguinea, J.; Martinezfrias, J.; Gonzalezmartin, R.; Zamora, L. Framboidal pyrites in antique books. *Nature* **1997**, *388*, 631. [[CrossRef](#)]
53. Wignall, P.B.; Newton, R. Pyrite framboid diameter as a measure of oxygen deficiency in ancient mudrocks. *Am. J. Sci.* **1998**, *298*, 537–552. [[CrossRef](#)]
54. Berner, R.A.; Raiswell, R. Burial of organic carbon and pyrite sulfur in sediments over phanerozoic time: A new theory. *Geochim. Cosmochim. Acta* **1983**, *47*, 855–862. [[CrossRef](#)]
55. Berner, R.A. Sedimentary pyrite formation: An update. *Geochim. Cosmochim. Acta* **1984**, *48*, 605–615. [[CrossRef](#)]
56. Bonnetti, C.; Liu, X.; Cuney, M.; Malartre, F.; Michels, R. The Uranium metallogenic cycle in the intracontinental Erian Basin, NE China: From source to deposit. *Miner. Resour. A Sustain. World* **2015**, *69*, 1–5.
57. Zhang, C. Geochemical interface for uranium ore fluids. *Acta Geol. Sichuan* **2005**, *25*, 86–91, (In Chinese with English Abstract).
58. Jin, R.S.; Zhang, C.J.; Feng, X.X.; Tao, C.; Zhu, Q.; Li, G.Y. The influence of fluid mixing on the mineralization of sandstone type uranium deposits. *Geol. Bull. China* **2013**, *33*, 354–358, (In Chinese with English Abstract).
59. Xie, H.; Jiao, Y.; Liu, Z.; Li, X.D.; Yi, C.; Rong, H.; Wan, L.L. Occurrence and enrichment mechanism of uranium ore minerals from sandstone-type uranium deposit, Northern Ordos Basin. *Earth Sci.* **2020**, *45*, 1531, (In Chinese with English Abstract).
60. Doinikova, O.A.; Solodov, I.N.; Chertok, M.B. Mineral composition of uranium ore at the Dalmatovo deposit, Russia. *Geol. Ore Depos.* **2009**, *51*, 486–495. [[CrossRef](#)]
61. Langmuir, D. Uranium solution-mineral equilibria at low temperatures with applications to sedimentary ore deposits. *Geochim. Cosmochim. Acta* **1978**, *42*, 547–569. [[CrossRef](#)]
62. Cai, Y.; Wang, H.; Wang, X.; He, K.; Zhang, S.; Wu, C. Formation conditions and main controlling factors of uranium in marine source rocks. *Adv. Earth Sci.* **2017**, *32*, 199–208, (In Chinese with English Abstract).
63. Wang, Y. *The Study of Sediments Adsorption of Uranium in Phosphorus-Enriched Water System*; Chengdu University of Technology: Chengdu, China, 2014; pp. 70–87, (In Chinese with English Abstract).
64. Wang, J. Discussion on geochemical characteristics, mechanism and prospecting model of gley type sandstone uranium mineralization- taking Redwell Uranium deposit as an example. *Uranium Geol.* **1998**, *14*, 20–25, (In Chinese with English Abstract).

65. Ding, W.; Shen, K. Epigenetic alteration of sedimentary rocks at hydrogenic uranium deposit. *Uranium Geol.* **2001**, *17*, 83–89, (In Chinese with English Abstract).
66. Cai, C.F.; Dong, H.L.; Li, H.T.; Xiao, X.; Ou, G.; Zhang, C. Mineralogical and geochemical evidence for coupled bacterial uranium mineralization and hydrocarbon oxidation in the Shashagetai deposit, NW China. *Chem. Geol.* **2007**, *236*, 167–179. [[CrossRef](#)]
67. Alessi, D.S.; Lezama-Pacheco, J.S.; Stubbs, J.E.; Janousch, M.; Bargar, J.R.; Persson, P.; Bernier-Latmani, R. The product of microbial uranium reduction includes multiple species with U(IV)—Phosphate coordination. *Geochim. Cosmochim. Acta* **2014**, *131*, 115–127. [[CrossRef](#)]
68. Newsome, L.; Morris, K.; Lloyd, J.R. The biogeochemistry and bioremediation of uranium and other priority radionuclides. *Chem. Geol.* **2014**, *363*, 164–184. [[CrossRef](#)]
69. Welch, S.A.; Taunton, A.E.; Banfield, J.F. Effect of microorganisms and microbial metabolites on apatite dissolution. *Geomicrobiol. J.* **2002**, *19*, 343–367. [[CrossRef](#)]
70. Hutchens, E.; Valsami-Jones, E.; Harouiya, N.; Chaïrat, C.; Oelkers, E.H.; McEldoney, S. An experimental investigation of the effect of bacillus megaterium on apatite dissolution. *Geomicrobiol. J.* **2006**, *23*, 177–182. [[CrossRef](#)]
71. Toyoda, K.; Nakamura, Y.; Masuda, A. Rare earth elements of Pacific pelagic sediments. *Geochim. Cosmochim. Acta* **1990**, *54*, 1093–1103. [[CrossRef](#)]
72. Wei, J.; Tang, C.; Xu, Z.; Chen, L.; Guo, H.; Miao, P.; Du, S.; Zeng, H. Uranium mineral occurrence of the uraniferous rock series in Longhupao region, northern Songliao Basin. *Acta Mineral. Sin.* **2019**, *39*, 17, (In Chinese with English Abstract).
73. Gupta, D.K.; Walther, C. *Uranium in Plants and the Environment*; Springer: Berlin/Heidelberg, Germany, 2020; pp. 1–246.
74. Catalano, J.G.; Brown, J.R.G.E. Uranyl adsorption onto montmorillonite: Evaluation of binding sites and carbonate complexation. *Geochim. Cosmochim. Acta* **2005**, *69*, 2995–3005. [[CrossRef](#)]

Disclaimer/Publisher’s Note: The statements, opinions and data contained in all publications are solely those of the individual author(s) and contributor(s) and not of MDPI and/or the editor(s). MDPI and/or the editor(s) disclaim responsibility for any injury to people or property resulting from any ideas, methods, instructions or products referred to in the content.